Comparing Nonlinear Adaptive Motion Controllers for Marine Surface Vessels

Mikkel Eske Nørgaard Sørensen Morten Breivik

Centre for Autonomous Marine Operations and Systems, Department of Engineering Cybernetics, Norwegian University of Science and Technology, NO-7491 Trondheim, Norway
E-mail: mikkel.sorensen@itk.ntnu.no, morten.breivik@ieee.org

Abstract: This paper deals with the design and evaluation of four controllers based on backstepping and different adaptive control schemes, which are applied to the motion control of a nonlinear 3 degrees-of-freedom model of a marine surface vessel. The goal is to make a comparative analysis of the controllers in order to find out which one has the best performance. The considered controllers are: Adaptive backstepping, adaptive backstepping with command governor, $\mathcal{L}_1$ adaptive backstepping and $\mathcal{L}_1$ adaptive backstepping with command governor. Numerical simulations are performed for target tracking along both straight-line and circular paths, with uncertain model parameters and an unknown disturbance. Motion control performance is evaluated by performance metrics such as IAE, ISE, ITAE and a novel metric named IAEW which combines control accuracy and energy use in one single metric.

Keywords: Marine surface vessel, Nonlinear motion control, Adaptive backstepping, $\mathcal{L}_1$ adaptive backstepping, Command governor, Performance metrics

1. INTRODUCTION

Automated motion control of marine surface vessels has been a research topic since the early 20th century. In recent years, the research has expanded from control of manned vessels to also include unmanned vessels. When dealing with surface vessels in general, uncertain nonlinear hydrodynamics and external disturbances must be considered. To minimise uncertainties, experiments can be conducted to find the hydrodynamical coefficients. Changes in coefficients nevertheless occur. Also, external disturbances are difficult or impossible to measure. Adaptive control methods can be employed to deal with such uncertainties such that the vessel can still achieve its control objectives.

Even though the field of adaptive control dates back to the early 1950s, it has experienced an increased amount of interest and research effort during the last decade. This effort has lead to some new and promising control techniques such as $\mathcal{L}_1$ adaptive control (Hovakimyan and Cao, 2010) and the novel command governor architecture for adaptive stabilization and command following (Yucelen and Johnson, 2012a).

The $\mathcal{L}_1$ adaptive control method has been used in many fields, especially within aerial applications (Patel et al., 2007), where parameters can change very rapidly. However, it has still not been widely used for motion control of marine vessels. Examples include (Breu and Fossen, 2011), where $\mathcal{L}_1$ adaptive control was applied to deal with the parametric resonance problem for ships. In (Svendsen et al., 2012), an adaptive robust control system was developed to govern the steering of a high-speed unmanned watercraft maintaining uniform performance across the operational envelope. Based on these results, the authors in (Theisen et al., 2013) developed an $\mathcal{L}_1$ adaptive hovering control of an unmanned watercraft in a station-keeping mode. In addition, (Ren et al., 2014) used $\mathcal{L}_1$ adaptive control to improve the steering of a surface vessel along a predefined path.

In (Yucelen and Johnson, 2012a), a linear command governor was combined with the model reference adaptive control method to improve transient performance. In (Yucelen and Johnson, 2012b), a lowpass filter was applied to achieve a more robust adaptive control solution. Also, constrained adaptive control was combined with the command governor in (Schatz et al., 2013).

This paper will compare and evaluate the performance of the adaptive backstepping control method (Krstic et al., 1995) and the $\mathcal{L}_1$ adaptive backstepping control method applied to nonlinear motion control of marine surface vessels. In addition, it will be investigated if it is possible to improve the performance of these control methods by combining them with a modified command governor architecture.

The structure of this paper is as follows: A mathematical model and assumptions are presented in Section 2; Section 3 presents the design of the adaptive control laws applied to the vessel model; Section 4 includes simulation results and performance evaluation; while Section 5 concludes the paper.

2. SURFACE VESSEL MODEL

The motion of a surface vessel can be represented by the pose vector $\boldsymbol{\eta} = [x, y, \psi]^\top \in \mathbb{R}^2 \times \mathbb{S}$ and the velocity vector $\boldsymbol{\nu} = [u, v, r]^\top \in \mathbb{R}^3$, where $\mathbb{S} \in [-\pi, \pi]$. Here, (x, y)

represents the Cartesian position in the local reference frame, ψ is the yaw angle, (u, v) represents the body-fixed linear velocities and r is the yaw rate.

The 3 DOF dynamics of a surface vessel can be stated as (Fossen, 2011):

$$\dot{\boldsymbol{\eta}} = \mathbf{R}(\psi)\boldsymbol{\nu} \tag{1}$$

$$\boldsymbol{M^*}\dot{\boldsymbol{\nu}} + \boldsymbol{C^*}(\boldsymbol{\nu})\boldsymbol{\nu} + \boldsymbol{D^*}(\boldsymbol{\nu})\boldsymbol{\nu} = \boldsymbol{\tau^*} + \mathbf{R}^\top(\psi)\boldsymbol{w}^*, \tag{2}$$

where

$$\mathbf{R}(\psi) = \begin{bmatrix} \cos(\psi) & -\sin(\psi) & 0 \\ \sin(\psi) & \cos(\psi) & 0 \\ 0 & 0 & 1 \end{bmatrix} \tag{3}$$

is a rotation matrix $\mathbf{R} \in SO(3)$, and where $\mathbf{M}^*$, $\boldsymbol{C^*}(\boldsymbol{\nu})$, $\boldsymbol{D^*}(\boldsymbol{\nu})$, $\boldsymbol{\tau^*}$ and $\boldsymbol{w}^*$ represent the real inertia matrix, Coriolis and centripetal matrix, damping matrix, control input vector and disturbance vector, respectively. Here, the system matrices are assumed to satisfy the properties $\mathbf{M}^* = \mathbf{M}^{*\top} > 0$, $\mathbf{C}^*(\boldsymbol{\nu}) = -\mathbf{C}^*(\boldsymbol{\nu})^\top$ and $\mathbf{D}^*(\boldsymbol{\nu}) > 0$.

However, there are uncertainties associated with the real matrices and vectors. Therefore, we assume that the relationship between the real and considered system matrices is parametrised as

$$\mathbf{M}^* = \delta\mathbf{M}, \tag{4}$$

$$\boldsymbol{C^*}(\boldsymbol{\nu}) = \delta\boldsymbol{C}(\boldsymbol{\nu}), \tag{5}$$

$$\boldsymbol{D^*}(\boldsymbol{\nu}) = \sigma\boldsymbol{D}(\boldsymbol{\nu}), \tag{6}$$

$$\boldsymbol{\tau^*} = \rho\boldsymbol{\tau}, \tag{7}$$

where $\delta \in \mathbb{R}^+$ is the uncertainty associated with the inertia matrix, $\sigma \in \mathbb{R}^+$ is the uncertainty associated with the damping matrix and $\rho \in \mathbb{R}^+$ is the uncertainty associated with the control input vector. Additionally, it is assumed that $\dot{\delta} = 0$, $\dot{\sigma} = 0$, $\dot{\rho} = 0$ and $\dot{\boldsymbol{w}}^* = \mathbf{0}$, i.e., that the uncertainties and disturbance are constant or slowly varying relative to the vessel dynamics.

Applying (4)-(7) into (2), the vessel model can also be stated as

$$\dot{\boldsymbol{\eta}} = \mathbf{R}(\psi)\boldsymbol{\nu} \tag{8}$$

$$\delta[\mathbf{M}\dot{\boldsymbol{\nu}} + \mathbf{C}(\boldsymbol{\nu})\boldsymbol{\nu}] + \sigma\mathbf{D}(\boldsymbol{\nu})\boldsymbol{\nu} = \rho\boldsymbol{\tau} + \mathbf{R}^\top(\psi)\boldsymbol{w}^*. \tag{9}$$

3. NONLINEAR ADAPTIVE MOTION CONTROLLERS

In this section, a step-by-step design procedure for the different nonlinear adaptive motion controllers will be presented. It is assumed that both the pose vector $\boldsymbol{\eta}$ and velocity vector $\boldsymbol{\nu}$ can be measured. In addition, it is assumed that there are no magnitude or rate saturations for the control input $\boldsymbol{\tau}^*$.

The control objective is to make $|\boldsymbol{\eta}(t) - \boldsymbol{\eta}_d(t)| \to 0$, where $\boldsymbol{\eta}_d(t)$ is $\mathcal{C}^2$ and bounded. This reference signal is typically defined by a human or generated by a guidance system.

3.1 Adaptive Backstepping

The design approach of an adaptive backstepping controller is divided into several stages, including the definition of new state variables, finding the control law through control Lyapunov functions (CLF) and designing the adaptation laws. For notational simplicity, the time t is omitted. The design procedure of this approach is inspired by (Krstic et al., 1995), (Fossen and Strand, 1999) and (Fossen, 2011).

Start by defining the error variables $\mathbf{z}_1$ and $\mathbf{z}_2$:

$$\mathbf{z}_1 \triangleq \mathbf{R}^\top(\psi)(\boldsymbol{\eta} - \boldsymbol{\eta}_d) \tag{10}$$

$$\mathbf{z}_2 \triangleq \boldsymbol{\nu} - \boldsymbol{\alpha}, \tag{11}$$

where $\boldsymbol{\alpha} \in \mathbb{R}^3$ is a vector of stabilising functions to be designed.

Step 1:
Choosing a positive definite (CLF)

$$V_1 = \frac{1}{2}\mathbf{z}_1^\top\mathbf{z}_1, \tag{12}$$

the derivative of V_1 with respect to (w.r.t) time along the $\mathbf{z}_1$-dynamics gives

$$\begin{aligned}\dot{V}_1 &= \mathbf{z}_1^\top\dot{\mathbf{z}}_1 \\ &= \mathbf{z}_1^\top(\mathbf{S}(r)^\top\mathbf{R}^\top(\psi)(\boldsymbol{\eta} - \boldsymbol{\eta}_d) + \mathbf{R}^\top(\psi)(\dot{\boldsymbol{\eta}} - \dot{\boldsymbol{\eta}}_d)) \\ &= \mathbf{z}_1^\top(\mathbf{S}(r)^\top\mathbf{z}_1 + \mathbf{R}^\top(\psi)(\dot{\boldsymbol{\eta}} - \dot{\boldsymbol{\eta}}_d)),\end{aligned}$$

where

$$\mathbf{S}(r) = \begin{bmatrix} 0 & -r & 0 \\ r & 0 & 0 \\ 0 & 0 & 0 \end{bmatrix},$$

and by applying the skew-symmetric property $\mathbf{z}_1^\top\mathbf{S}(r)^\top\mathbf{z}_1 = 0$, gives

$$\dot{V}_1 = \mathbf{z}_1^\top(\boldsymbol{\nu} - \mathbf{R}^\top(\psi)\dot{\boldsymbol{\eta}}_d).$$

Using (11), the CLF becomes

$$\begin{aligned}\dot{V}_1 &= \mathbf{z}_1^\top(\mathbf{z}_2 + \boldsymbol{\alpha} - \mathbf{R}^\top(\psi)\dot{\boldsymbol{\eta}}_d) \\ &= \mathbf{z}_1^\top\mathbf{z}_2 + \mathbf{z}_1^\top(\boldsymbol{\alpha} - \mathbf{R}^\top(\psi)\dot{\boldsymbol{\eta}}_d).\end{aligned}$$

The stabilising function can now be chosen as

$$\boldsymbol{\alpha} = \mathbf{R}^\top(\psi)\dot{\boldsymbol{\eta}}_d - \mathbf{K}_1\mathbf{z}_1, \tag{13}$$

where $\mathbf{K}_1 > 0$, which results in

$$\dot{V}_1 = -\mathbf{z}_1^\top\mathbf{K}_1\mathbf{z}_1 + \mathbf{z}_2^\top\mathbf{z}_1,$$

which concludes Step 1.

Step 2:
By defining

$$\delta_\rho \triangleq \frac{\delta}{\rho}, \quad \sigma_\rho \triangleq \frac{\sigma}{\rho}, \quad \boldsymbol{w}_\rho^* = \frac{1}{\rho}\boldsymbol{w}^*, \tag{14}$$

the $\mathbf{z}_2$ dynamics can be written as

$$\begin{aligned}\delta_\rho\mathbf{M}\dot{\mathbf{z}}_2 =& \delta_\rho\mathbf{M}(\dot{\boldsymbol{\nu}} - \dot{\boldsymbol{\alpha}}) \\ =& \boldsymbol{\tau} + \mathbf{R}^\top(\psi)\boldsymbol{w}_\rho^* - \delta_\rho\mathbf{C}(\boldsymbol{\nu})\boldsymbol{\nu} - \sigma_\rho\mathbf{D}(\boldsymbol{\nu})\boldsymbol{\nu} - \delta_\rho\mathbf{M}\dot{\boldsymbol{\alpha}},\end{aligned}$$

where

$$\dot{\boldsymbol{\alpha}} = \mathbf{R}^\top(\psi)\ddot{\boldsymbol{\eta}}_d + \mathbf{S}(r)^\top\mathbf{R}^\top(\psi)\dot{\boldsymbol{\eta}}_d - \mathbf{K}_1\dot{\mathbf{z}}_1.$$

By including both $\mathbf{z}_1$ and $\mathbf{z}_2$, the CLF is modified to

$$V_2 = \frac{1}{2}\mathbf{z}_2^\top\delta_\rho\mathbf{M}\mathbf{z}_2 + V_1. \tag{15}$$

Rewriting $\mathbf{C}(\boldsymbol{\nu}) = \mathbf{C}$, $\mathbf{D}(\boldsymbol{\nu}) = \mathbf{D}$ and $\mathbf{R}(\psi) = \mathbf{R}$ for notational brevity, the derivative of this CLF is

$$\begin{aligned}\dot{V}_2 =& \mathbf{z}_2^\top\delta_\rho\mathbf{M}\dot{\mathbf{z}}_2 + \dot{V}_1, \\ =& \mathbf{z}_2^\top[\boldsymbol{\tau} + \mathbf{R}^\top\boldsymbol{w}_\rho^* - \delta_\rho\mathbf{C}\boldsymbol{\nu} - \sigma_\rho\mathbf{D}\boldsymbol{\nu} - \delta_\rho\mathbf{M}\dot{\boldsymbol{\alpha}}] \\ & - \mathbf{z}_1^\top\mathbf{K}_1\mathbf{z}_1 + \mathbf{z}_2^\top\mathbf{z}_1.\end{aligned}$$

Utilising the fact that $\boldsymbol{\nu} = \mathbf{z}_2 + \boldsymbol{\alpha}$, we obtain

$$\begin{aligned}\dot{V}_2 =& \mathbf{z}_2^\top[\mathbf{z}_1 + \boldsymbol{\tau} + \mathbf{R}^\top\boldsymbol{w}_\rho^* - \delta_\rho\mathbf{C}\boldsymbol{\alpha} - \sigma_\rho\mathbf{D}\boldsymbol{\alpha} - \delta_\rho\mathbf{M}\dot{\boldsymbol{\alpha}}] \\ & - \mathbf{z}_1^\top\mathbf{K}_1\mathbf{z}_1 - \mathbf{z}_2^\top\delta_\rho\mathbf{C}\mathbf{z}_2 - \mathbf{z}_2^\top\sigma_\rho\mathbf{D}\mathbf{z}_2.\end{aligned}$$

Applying the skew-symmetric property $\mathbf{z}_2^\top \delta_\rho \mathbf{C}\mathbf{z}_2 = 0$, yields

$$\begin{aligned}\dot{V}_2 =&\mathbf{z}_2^\top[\mathbf{z}_1 + \boldsymbol{\tau} + \mathbf{R}^\top \boldsymbol{w}_\rho^* - \delta_\rho \mathbf{C}\boldsymbol{\alpha} - \sigma_\rho \mathbf{D}\boldsymbol{\alpha} - \delta_\rho \mathbf{M}\dot{\boldsymbol{\alpha}}] \\ &- \mathbf{z}_1^\top \mathbf{K}_1 \mathbf{z}_1 - \mathbf{z}_2^\top \sigma_\rho \mathbf{D}\mathbf{z}_2.\end{aligned}$$

The control law can be chosen as

$$\begin{aligned}\boldsymbol{\tau} =& -\mathbf{R}^\top \boldsymbol{w}_\rho^* + \delta_\rho[\mathbf{M}\dot{\boldsymbol{\alpha}} + \mathbf{C}\boldsymbol{\alpha}] + \sigma_\rho \mathbf{D}\boldsymbol{\alpha} \\ &- \mathbf{z}_1 - \mathbf{K}_2\mathbf{z}_2,\end{aligned} \tag{16}$$

where $\mathbf{K}_2 > 0$. This results in

$$\dot{V}_2 = -\mathbf{z}_1^\top \mathbf{K}_1 \mathbf{z}_1 - \mathbf{z}_2^\top(\mathbf{K}_2 + \sigma_\rho \mathbf{D})\mathbf{z}_2 \leq 0.$$

Step 3:
The parameters δ_ρ, σ_ρ and $\boldsymbol{w}_\rho^*$ are not known in the control laws in (16), and the CLF is expanded to

$$V_3 = \frac{1}{2}\left[\frac{1}{\gamma_{\delta_\rho}}\tilde{\delta}_\rho^2 + \frac{1}{\gamma_{\sigma_\rho}}\tilde{\sigma}_\rho^2 + \frac{1}{\gamma_{w_\rho}}\tilde{\boldsymbol{w}}_\rho{}^\top \tilde{\boldsymbol{w}}_\rho\right] + V_2, \tag{17}$$

where γ_{δ_ρ}, γ_{σ_ρ} and γ_{w_ρ} are the adaptation gains. Also, $\tilde{\delta}_\rho \triangleq \hat{\delta}_\rho - \delta_\rho$, $\tilde{\sigma}_\rho \triangleq \hat{\sigma}_\rho - \sigma_\rho$, $\tilde{\boldsymbol{w}}_\rho \triangleq \hat{\boldsymbol{w}}_\rho - \boldsymbol{w}_\rho^*$. The derivative of V_3 then becomes

$$\begin{aligned}\dot{V}_3 =&\frac{1}{\gamma_{\delta_\rho}}\tilde{\delta}_\rho\dot{\tilde{\delta}}_\rho + \frac{1}{\gamma_{\sigma_\rho}}\tilde{\sigma}_\rho\dot{\tilde{\sigma}}_\rho + \frac{1}{\gamma_{w_\rho}}\tilde{\boldsymbol{w}}_\rho{}^\top \dot{\tilde{\boldsymbol{w}}}_\rho + \mathbf{z}_2^\top[\tilde{\delta}_\rho(\mathbf{M}\dot{\boldsymbol{\alpha}} + \mathbf{C}\boldsymbol{\alpha}) \\ &+ \tilde{\sigma}_\rho(\mathbf{D}\boldsymbol{\alpha}) - (\mathbf{K}_2 + \sigma_\rho\mathbf{D})\mathbf{z}_2 - \mathbf{R}^\top\tilde{\boldsymbol{w}}_\rho] - \mathbf{z}_1^\top\mathbf{K}_1\mathbf{z}_1.\end{aligned}$$

To eliminate the uncertainty terms $\tilde{\delta}_\rho$ and $\tilde{\sigma}_\rho$, the update laws are chosen as

$$\dot{\tilde{\delta}}_\rho = -\gamma_{\delta_\rho}\mathbf{z}_2^\top[\mathbf{M}\dot{\boldsymbol{\alpha}} + \mathbf{C}\boldsymbol{\alpha}], \tag{18}$$

$$\dot{\tilde{\sigma}}_\rho = -\gamma_{\sigma_\rho}\mathbf{z}_2^\top\mathbf{D}\boldsymbol{\alpha}, \tag{19}$$

$$\dot{\tilde{\boldsymbol{w}}}_\rho = \gamma_{w_\rho}\mathbf{R}\mathbf{z}_2, \tag{20}$$

which results in

$$\dot{V}_3 = -\mathbf{z}_1^\top\mathbf{K}_1\mathbf{z}_1 - \mathbf{z}_2^\top\mathbf{K}_2\mathbf{z}_2 \leq 0, \quad \forall \mathbf{z}_1, \mathbf{z}_2 \neq 0.$$

It can be concluded that the origin of the error system $(\mathbf{z}_1, \mathbf{z}_2, \tilde{\delta}_\rho, \tilde{\sigma}_\rho, \tilde{\boldsymbol{w}}_\rho)$ is uniformly globally asymptotically stable (UGAS) by utilising Theorem A.6 from (Fossen, 2011).

3.2 $\mathcal{L}_1$ Adaptive Backstepping

The design of the $\mathcal{L}_1$ adaptive backstepping controller is divided into two stages. The first stage concerns design of the adaptation laws and the second stage of the control law, inspired by the approach in (Lee et al., 2012).

State Predictor and Adaptation Laws
First, a state predictor is designed, where the prediction errors are defined as

$$\tilde{\boldsymbol{\eta}} \triangleq \hat{\boldsymbol{\eta}} - \boldsymbol{\eta}, \quad \tilde{\boldsymbol{\nu}} \triangleq \hat{\boldsymbol{\nu}} - \boldsymbol{\nu}, \tag{21}$$

where $\hat{\boldsymbol{\eta}}$, $\hat{\boldsymbol{\nu}}$, $\boldsymbol{\eta}$ and $\boldsymbol{\nu}$ represent the estimated pose, estimated velocity, real pose and real velocity, respectively. The ideal prediction error dynamics are chosen to be

$$\dot{\tilde{\boldsymbol{\eta}}}_{ideal} = -\mathbf{L}_1\tilde{\boldsymbol{\eta}}, \quad \dot{\tilde{\boldsymbol{\nu}}}_{ideal} = -\mathbf{L}_2\tilde{\boldsymbol{\nu}},$$

where $\mathbf{L}_1 > 0$ and $\mathbf{L}_2 > 0$, such that their origins are exponentially stable. The convergence rate is decided through the positive definite gain matrices. The state predictor dynamics becomes

$$\dot{\hat{\boldsymbol{\eta}}} = -\mathbf{L}_1\tilde{\boldsymbol{\eta}} + \mathbf{R}\boldsymbol{\nu}, \tag{22}$$

$$\dot{\hat{\boldsymbol{\nu}}} = -\mathbf{L}_2\tilde{\boldsymbol{\nu}} + \mathbf{M}^{-1}(\hat{\rho}_\delta\boldsymbol{\tau} + \mathbf{R}^\top\hat{\boldsymbol{w}}_\delta - \mathbf{C}\boldsymbol{\nu} - \hat{\sigma}_\delta\mathbf{D}\boldsymbol{\nu}), \tag{23}$$

where $\hat{\sigma}_\delta \triangleq \frac{\hat{\sigma}}{\hat{\delta}}$, $\hat{\rho}_\delta \triangleq \frac{\hat{\rho}}{\hat{\delta}}$, $\hat{\boldsymbol{w}}_\delta \triangleq \frac{1}{\hat{\delta}}\hat{\boldsymbol{w}}$, and $\hat{\sigma}$, $\hat{\rho}$ and $\hat{\delta}$ are estimates of the damping, control input and inertia uncertainties. Here, it is assumed that $\hat{\delta} \in \mathbb{R}^+$. The dynamics of $\hat{\sigma}_\delta$, $\hat{\rho}_\delta$ and $\hat{\boldsymbol{w}}_\delta$ must subsequently be designed.

It is desired to design adaptation laws for the uncertainties. The derivation of these laws are based on Lyapunov functions. However, the prediction error dynamics are first defined as

$$\dot{\tilde{\boldsymbol{\eta}}} = -\mathbf{L}_1\tilde{\boldsymbol{\eta}}, \tag{24}$$

$$\dot{\tilde{\boldsymbol{\nu}}} = -\mathbf{L}_2\tilde{\boldsymbol{\nu}} + \mathbf{M}^{-1}(\tilde{\rho}_\delta\boldsymbol{\tau} + \mathbf{R}^\top\tilde{\boldsymbol{w}}_\delta - \tilde{\sigma}_\delta\mathbf{D}\boldsymbol{\nu}). \tag{25}$$

Then consider the positive definite CLF

$$\begin{aligned}V_{pred} =&\frac{1}{2}\left(\frac{1}{\gamma_{\rho_\delta}}\tilde{\rho}_\delta^2 + \frac{1}{\gamma_{\sigma_\delta}}\tilde{\sigma}_\delta^2 + \frac{1}{\gamma_{w_\delta}}\tilde{\boldsymbol{w}}_\delta{}^\top\tilde{\boldsymbol{w}}_\delta\right) \\ &+ \frac{1}{2}\tilde{\boldsymbol{\nu}}^\top\mathbf{M}\tilde{\boldsymbol{\nu}} + \frac{1}{2}\tilde{\boldsymbol{\eta}}^\top\tilde{\boldsymbol{\eta}}.\end{aligned} \tag{26}$$

Taking the derivative of (26) yields

$$\begin{aligned}\dot{V}_{pred} =&\frac{1}{\gamma_{\rho_\delta}}\tilde{\rho}_\delta\dot{\tilde{\rho}}_\delta + \frac{1}{\gamma_{\sigma_\delta}}\tilde{\sigma}_\delta\dot{\tilde{\sigma}}_\delta + \frac{1}{\gamma_{w_\delta}}\tilde{\boldsymbol{w}}_\delta{}^\top\dot{\tilde{\boldsymbol{w}}}_\delta - \tilde{\boldsymbol{\eta}}^\top\mathbf{L}_1\tilde{\boldsymbol{\eta}} \\ &+ \tilde{\boldsymbol{\nu}}^\top(-\mathbf{M}\mathbf{L}_2\tilde{\boldsymbol{\nu}} + \tilde{\rho}_\delta\boldsymbol{\tau} + \mathbf{R}^\top\tilde{\boldsymbol{w}}_\delta - \tilde{\sigma}_\delta\mathbf{D}\boldsymbol{\nu}) \\ =&\tilde{\rho}_\delta\left(\frac{1}{\gamma_{\rho_\delta}}\dot{\hat{\rho}}_\delta + \tilde{\boldsymbol{\nu}}^\top\boldsymbol{\tau}\right) + \tilde{\sigma}_\delta\left(\frac{1}{\gamma_{\sigma_\delta}}\dot{\hat{\sigma}}_\delta - \tilde{\boldsymbol{\nu}}^\top\mathbf{D}\boldsymbol{\nu}\right) \\ &+ \tilde{\boldsymbol{w}}_\delta{}^\top\left(\frac{1}{\gamma_{w_\delta}}\dot{\hat{\boldsymbol{w}}}_\delta + \mathbf{R}\tilde{\boldsymbol{\nu}}\right) + \tilde{\boldsymbol{\nu}}^\top(-\mathbf{M}\mathbf{L}_2\tilde{\boldsymbol{\nu}}) \\ &- \tilde{\boldsymbol{\eta}}^\top\mathbf{L}_1\tilde{\boldsymbol{\eta}}.\end{aligned} \tag{27}$$

By introducing the following adaptation laws

$$\dot{\hat{\rho}}_\delta = -\gamma_{\rho_\delta}\tilde{\boldsymbol{\nu}}^\top\boldsymbol{\tau}, \tag{28}$$

$$\dot{\hat{\sigma}}_\delta = \gamma_{\sigma_\delta}\tilde{\boldsymbol{\nu}}^\top\mathbf{D}\boldsymbol{\nu}, \tag{29}$$

$$\dot{\hat{\boldsymbol{w}}}_\delta = -\gamma_{w_\delta}\mathbf{R}\tilde{\boldsymbol{\nu}}, \tag{30}$$

then (27) becomes

$$\dot{V}_{pred} = -\tilde{\boldsymbol{\eta}}^\top\mathbf{L}_1\tilde{\boldsymbol{\eta}} - \tilde{\boldsymbol{\nu}}^\top\mathbf{M}\mathbf{L}_2\tilde{\boldsymbol{\nu}} \leq 0, \quad \forall \boldsymbol{\eta}, \boldsymbol{\nu} \neq 0.$$

Control Law
By following Step 1 and 2 in the design procedure of adaptive backstepping, the control law is derived through the following CLF

$$V_{ctrl} = \frac{1}{2}\mathbf{z}_2^\top\mathbf{M}\mathbf{z}_2 + \frac{1}{2}\mathbf{z}_1^\top\mathbf{z}_1, \tag{31}$$

where the derivative is

$$\begin{aligned}\dot{V}_{ctrl} =&\mathbf{z}_2^\top[\mathbf{z}_1 + \hat{\rho}_\delta\boldsymbol{\tau} + \mathbf{R}^\top\hat{\boldsymbol{w}}_\delta - \mathbf{C}\boldsymbol{\alpha} - \hat{\sigma}_\delta\mathbf{D}\boldsymbol{\alpha} - \mathbf{M}\dot{\boldsymbol{\alpha}}] \\ &- \mathbf{z}_1^\top\mathbf{K}_1\mathbf{z}_1 - \mathbf{z}_2^\top\hat{\sigma}_\delta\mathbf{D}\mathbf{z}_2\end{aligned} \tag{32}$$

and chosen to be

$$\begin{aligned}\hat{\rho}_\delta\boldsymbol{\tau} =& -\mathbf{R}^\top\hat{\boldsymbol{w}}_\delta + \mathbf{M}\dot{\boldsymbol{\alpha}} + \mathbf{C}\boldsymbol{\alpha} + \hat{\sigma}_\delta\mathbf{D}\boldsymbol{\alpha} \\ &- \mathbf{z}_1 - \mathbf{K}_2\mathbf{z}_2,\end{aligned} \tag{33}$$

which leads to

$$\dot{V}_{ctrl} = -\mathbf{z}_1^\top\mathbf{K}_1\mathbf{z}_1 - \mathbf{z}_2^\top\mathbf{K}_2\mathbf{z}_2 \leq 0, \quad \forall \mathbf{z}_1, \mathbf{z}_2 \neq 0. \tag{34}$$

The adaptation of the uncertainties may contain high-frequency signals. To avoid introducing such frequencies into the control input, a lowpass filter is applied to the control signals such that

$$\boldsymbol{\tau}_c = C(s)\boldsymbol{\tau},$$

where

$$C(s) = \frac{\hat{\rho}_0 k}{s + \hat{\rho}_0 k}$$

and the gain $k > 0$ represents the design parameter of the lowpass filter, while $\hat{\rho}_0 = \hat{\rho}(0)$ is the initial guess of ρ.

3.3 Adding a Command Governor

The idea of making a virtual command signal seems to have originally been introduced in (Bemporad and Mosca, 1995). Recently, the papers by (Yucelen and Johnson, 2012a) and (Schatz et al., 2013) discuss a novel command governor algorithm to improve both transient and steady state tracking of a reference signal for the model reference adaptive control algorithm. However, the command governor in (Yucelen and Johnson, 2012a) is not directly applicable to nonlinear controllers. Hence, we propose the following dynamics for the command signal $\boldsymbol{\eta}_i$ as

$$\dot{\boldsymbol{\eta}}_i \triangleq \dot{\boldsymbol{\eta}}_d - \mathbf{K}_a(\boldsymbol{\eta} - \boldsymbol{\eta}_i) + \mathbf{K}_b(\boldsymbol{\eta}_d - \boldsymbol{\eta}_i), \tag{35}$$

and

$$\ddot{\boldsymbol{\eta}}_i = \ddot{\boldsymbol{\eta}}_d - \mathbf{K}_a(\dot{\boldsymbol{\eta}} - \dot{\boldsymbol{\eta}}_i) + \mathbf{K}_b(\dot{\boldsymbol{\eta}}_d - \dot{\boldsymbol{\eta}}_i), \tag{36}$$

where $\mathbf{K}_b > \mathbf{K}_a > 0$ and the initial condition of the command governor is $\boldsymbol{\eta}_{i,0} = \boldsymbol{\eta}_0$.

Using the command governor means that

$$\mathbf{z}_1 \triangleq \mathbf{R}^\top(\boldsymbol{\eta} - \boldsymbol{\eta}_i), \tag{37}$$

which means that the vessel tracks an intermediate pose $\boldsymbol{\eta}_i$, which tracks the desired pose $\boldsymbol{\eta}_d$, in order to improve transient control performance.

By choosing the CLF

$$V_0 = \frac{1}{2}\mathbf{z}_0^\top \mathbf{z}_0, \tag{38}$$

where

$$\mathbf{z}_0 = \boldsymbol{\eta}_i - \boldsymbol{\eta}_d, \tag{39}$$

the derivative of V_0 will be

$$\begin{aligned}\dot{V}_0 &= \mathbf{z}_0^\top(-\mathbf{K}_a(\boldsymbol{\eta} - \boldsymbol{\eta}_i) - \mathbf{K}_b(\boldsymbol{\eta}_i - \boldsymbol{\eta}_d)) \\ &= \mathbf{z}_0^\top(-\mathbf{K}_a(\boldsymbol{\eta} - \boldsymbol{\eta}_i) - \mathbf{K}_b\mathbf{z}_0) \\ &= \mathbf{z}_0^\top(-\mathbf{K}_a\mathbf{R}\mathbf{z}_1 - \mathbf{K}_b\mathbf{z}_0) \\ &= -\mathbf{z}_0^\top\mathbf{K}_a\mathbf{R}\mathbf{z}_1 - \mathbf{z}_0^\top\mathbf{K}_b\mathbf{z}_0 \end{aligned} \tag{40}$$

To cancel the term $-\mathbf{z}_0^\top\mathbf{K}_a\mathbf{R}\mathbf{z}_1$, the stabilising function $\boldsymbol{\alpha}$ is altered to be

$$\boldsymbol{\alpha} = \mathbf{R}^\top\dot{\boldsymbol{\eta}}_i + \mathbf{R}^\top\mathbf{K}_a\mathbf{z}_0 - \mathbf{K}_1\mathbf{z}_1, \tag{41}$$

which means that

$$\dot{\boldsymbol{\alpha}} = \mathbf{R}^\top\ddot{\boldsymbol{\eta}}_i + \mathbf{S}^\top\mathbf{R}^\top\dot{\boldsymbol{\eta}}_i + \mathbf{R}^\top\mathbf{K}_a\dot{\mathbf{z}}_0 + \mathbf{S}^\top\mathbf{R}^\top\mathbf{K}_a\mathbf{z}_0 - \mathbf{K}_1\dot{\mathbf{z}}_1 \tag{42}$$

Hence, introduction of the command governor does not change the stability of the closed-loop system. A general schematic of the proposed adaptive controller scheme with command governor is displayed in Fig. 1.

4. SIMULATION RESULTS AND PERFORMANCE EVALUATION

This section starts with the structure and parameters of the vessel model, followed by the initial states and control parameters used in the simulations. Subsequently, the metrics used to evaluate the performance are stated. Finally, the results associated with the different controllers are presented and discussed. For simulation purposes, the controllers are implemented in Matlab.

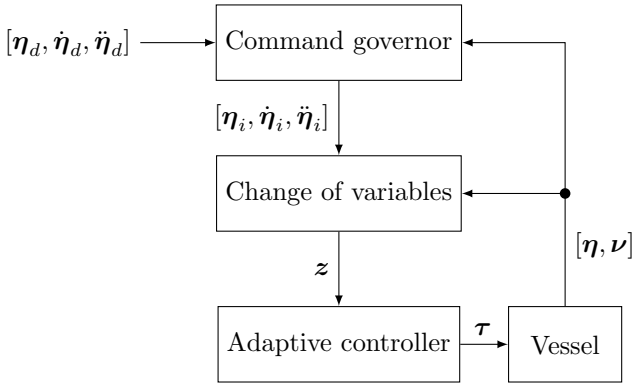

Fig. 1. Schematic of the command governor principle

4.1 Simulation Setup

Vessel Model Parameters
The model ship CyberShip II from (Skjetne et al., 2004) will be used to verify the performance of the proposed adaptive control methods. CyberShip II is a 1:70 scale replica of a supply ship, with a length of $L = 1.255$ (m). It is fully actuated and can maximum produce 2 (N) in surge and sway.

The inertia matrix is given as

$$\mathbf{M}^* \triangleq \mathbf{M}_{RB} + \mathbf{M}_A,$$

where

$$\mathbf{M}_{RB} = \begin{bmatrix} m & 0 & 0 \\ 0 & m & mx_g \\ 0 & mx_g & I_z \end{bmatrix}, \quad \mathbf{M}_A = \begin{bmatrix} -X_{\dot{u}} & 0 & 0 \\ 0 & -Y_{\dot{v}} & -Y_{\dot{r}} \\ 0 & -N_{\dot{v}} & -N_{\dot{r}} \end{bmatrix},$$

and m represent the mass of the ship, while x_g is the distance along the x-axis in the body from the centre of gravity. As displayed in (5), the real Coriolis matrix has the same uncertainty as (4) since

$$\mathbf{C}^*(\boldsymbol{\nu}) \triangleq \mathbf{C}_{RB}(\boldsymbol{\nu}) + \mathbf{C}_A(\boldsymbol{\nu}),$$

with

$$\mathbf{C}_{RB}(\boldsymbol{\nu}) = \begin{bmatrix} 0 & 0 & -m(x_g r + v) \\ 0 & 0 & mu \\ m(x_g r + v) & -mu & 0 \end{bmatrix},$$

$$\mathbf{C}_A(\boldsymbol{\nu}) = \begin{bmatrix} 0 & 0 & c_{13}(\boldsymbol{\nu}) \\ 0 & 0 & c_{23}(\boldsymbol{\nu}) \\ -c_{13}(\boldsymbol{\nu}) & -c_{23}(\boldsymbol{\nu}) & 0 \end{bmatrix},$$

where $c_{13}(\boldsymbol{\nu}) = Y_{\dot{v}}v + \frac{1}{2}(N_{\dot{v}} + Y_{\dot{r}})r$ and $c_{23}(\boldsymbol{\nu}) = -X_{\dot{u}}u$. Finally, the damping matrix $\mathbf{D}^*(\boldsymbol{\nu})$ is given as

$$\mathbf{D}^*(\boldsymbol{\nu}) \triangleq \mathbf{D}_L + \mathbf{D}_{NL}(\boldsymbol{\nu}),$$

where

$$\mathbf{D}_L = \begin{bmatrix} -X_u & 0 & 0 \\ 0 & -Y_v & -Y_r \\ 0 & -N_v & -N_r \end{bmatrix},$$

$$\mathbf{D}_{NL}(\boldsymbol{\nu}) = \begin{bmatrix} -d_{11}(\boldsymbol{\nu}) & 0 & 0 \\ 0 & -d_{22}(\boldsymbol{\nu}) & -d_{23}(\boldsymbol{\nu}) \\ 0 & -d_{32}(\boldsymbol{\nu}) & -d_{33}(\boldsymbol{\nu}) \end{bmatrix},$$

where $d_{11}(\boldsymbol{\nu}) = X_{|u|u}|u| + X_{uuu}u^2$, $d_{22}(\boldsymbol{\nu}) = Y_{|v|v}|v| + Y_{|r|v}|r|$, $d_{23}(\boldsymbol{\nu}) = Y_{|v|r}|v| + Y_{|r|r}|r|$, $d_{32}(\boldsymbol{\nu}) = N_{|v|v}|v| + N_{|r|v}|r|$ and $d_{33}(\boldsymbol{\nu}) = N_{|v|r}|v| + N_{|r|r}|r|$. The parameter values are listed in Table 1.

m	23.8	$X_{\dot{u}}$	-2	$N_{\dot{v}}$	0
I_z	1.760	$Y_{\dot{v}}$	-10	$N_{\dot{r}}$	-1
x_g	0.046	$Y_{\dot{r}}$	0		
X_u	-0.72253	Y_v	-0.88965		
$X_{\|u\|u}$	-1.32742	$Y_{\|v\|v}$	-36.47287		
X_{uuu}	-5.86643	N_v	0.03130		
		$N_{\|v\|v}$	3.95645		
$Y_{\|r\|v}$	-0.805	$N_{\|r\|v}$	0.130		
Y_r	-7.250	N_r	-1.900		
$Y_{\|v\|r}$	-0.845	$Y_{\|v\|r}$	0.080		
$Y_{\|r\|r}$	-3.450	$N_{\|r\|r}$	-0.750		

Table 1. Parameters for CyberShip II from (Skjetne et al., 2004)

Reference Signal, Initial States and Control Parameters
For a straight-line path, the reference pose $\boldsymbol{\eta}_d(t)$ is derived from

$$\boldsymbol{\eta}_d(t) = [x_d(t), y_d(t), \varphi]^\top, \tag{43}$$

where

$$\begin{aligned} x_d(t) &= 1 + \omega t \cos(\varphi) \\ \dot{x}_d(t) &= \omega \cos(\varphi) \\ \ddot{x}_d(t) &= 0 \\ \dot{\omega} &= 0, \end{aligned}$$

and

$$\begin{aligned} y_d(t) &= \omega t \sin(\varphi) \\ \dot{y}_d(t) &= \omega \sin(\varphi) \\ \ddot{y}_d(t) &= 0. \end{aligned}$$

It is assumed that the reference target has a constant speed $\omega = 0.15\ (m/s)$. For the full scale vessel, this corresponds to $1.255\ m/s$ using the Bis scale (Fossen, 2011). It is desired to have a constant orientation of the path relative to the x-axis $\varphi = 0.9273\ (rad)$, which is equivalent to 53 (deg). The initial condition of the reference signal is chosen to be $\boldsymbol{\eta}_d(0) = [1\ (m), 0\ (m), 0.9273\ (rad)]^\top$.

The initial vessel states are chosen to be $\boldsymbol{\eta}_0 = [0.5\ (m), 0\ (m), \pi/4\ (rad)]^\top$ and $\boldsymbol{\nu}_0 = [0\ (m/s), 0\ (m/s), 0\ (rad/s)]^\top$.

The uncertainties for the system are chosen to be $\delta = 2$, $\sigma = 2$, $\rho = 0.7$ and $\boldsymbol{w}^* = [-0.3536\ (N), 0.3536\ (N), 0\ (Nm)]^\top$, which becomes active at $t = 150$ sec. Hence, the disturbance $\boldsymbol{w}^*$ has a magnitude of 0.5 (N) and direction of 135 (deg). The initial values for the estimated uncertainties are $\delta_0 = 1$, $\sigma_0 = 1$, $\rho_0 = 1$ and $\boldsymbol{w}_0 = [0, 0, 0]^\top$.

The adaptive backstepping control parameters are chosen as $\mathbf{K}_1 = diag([0.05,\ 0.05,\ 0.02])$, $\mathbf{K}_2 = diag([5,\ 7,\ 15])$, $\gamma_{\delta_\rho} = \gamma_{\sigma_\rho} = 40$ and $\gamma_{w_\rho} = 6$.

The $\mathcal{L}_1$ adaptive backstepping method has a lowpass filter integrated in the control law to reject high frequency oscillations in the estimation of the uncertainties. Utilising this benefit, the $\mathcal{L}_1$ adaptive backstepping control parameters are chosen as $\mathbf{K}_1 = diag([0.05,\ 0.05,\ 0.02])$, $\mathbf{K}_2 = diag([5,\ 7,\ 15])$, $\mathbf{L}_1 = \mathbf{L}_2 = 100\mathbf{I}$, $k = 100$, $\gamma_{\rho_\delta} = \gamma_{\sigma_\delta} = 40$ and $\gamma_{w_\delta} = 500$. Notice that the $\mathcal{L}_1$ adaptive backstepping method has higher adaptation gains than the adaptive backstepping method.

The command governor uses the gains $\mathbf{K}_a = [0.01,\ 0.01,\ 0.005]$ and $\mathbf{K}_b = [0.05,\ 0.05,\ 0.01]$.

Since it was assumed that there are no magnitude or rate saturations for the control input $\boldsymbol{\tau}^*$, the control parameters and adaptation gains were obtained after iterative tuning.

Performance Metrics
To evaluate and compare the performance of the different control algorithms, performance metrics must be used. These include the integral of the absolute error (IAE), integral of the square of the error (ISE) and integral of the absolute error multiplied by time (ITAE) for the cross-track error. The cross-track error e will be used, which can be calculated by

$$e = -\sin(\psi)(x - x_d) + \cos(\psi)(y - y_d). \tag{44}$$

The formula for the IAE is then given as

$$IAE(e) = \int_0^t |e| dt, \tag{45}$$

which simply describes the temporal evolution of the absolute value of the error without adding any weight to the error. The ISE is defined as

$$ISE(e) = \int_0^t e^2 dt \tag{46}$$

and penalises large errors more than smaller ones, indicating how good the particular algorithm is at eliminating large errors. The calculation of ITAE is given as

$$ITAE(e) = \int_0^t t|e| dt, \tag{47}$$

which penalises errors which have been present for a long time more heavily than those present at the beginning. ITAE will show if there is a stationary error present in the system.

Finally, a new evaluation criterion is proposed, namely the integral of the absolute error multiplied by the energy consumption (IAEW), which can be computed by

$$IAEW(e) = \int_0^t |e| dt \int_0^t P dt, \tag{48}$$

where

$$P = ||\boldsymbol{\nu}^\top \boldsymbol{\tau}|| \tag{49}$$

represents the mechanical power. IAEW thus indicates which control algorithm has the best tracking performance versus energy consumption, in one single metric.

4.2 Results for Straight-line Motion

In the following, AB, AB-CG, L1-AB and L1-AB-CG refer to adaptive backstepping, adaptive backstepping with command governor, $\mathcal{L}_1$ adaptive backstepping and $\mathcal{L}_1$ adaptive backstepping with command governor, respectively.

Fig. 2 displays the desired path and the actual trajectory of the vessel in a North-East plot.

Fig. 3 illustrates the cross-track error of the methods scaled by the vessel length. The results of this figure show that all the methods have good tracking performance both with and without the presence of a disturbance. However, the $\mathcal{L}_1$ adaptive backstepping methods are faster to track the predefined trajectory and compensate for the disturbance, but overshoot the trajectory somewhat.

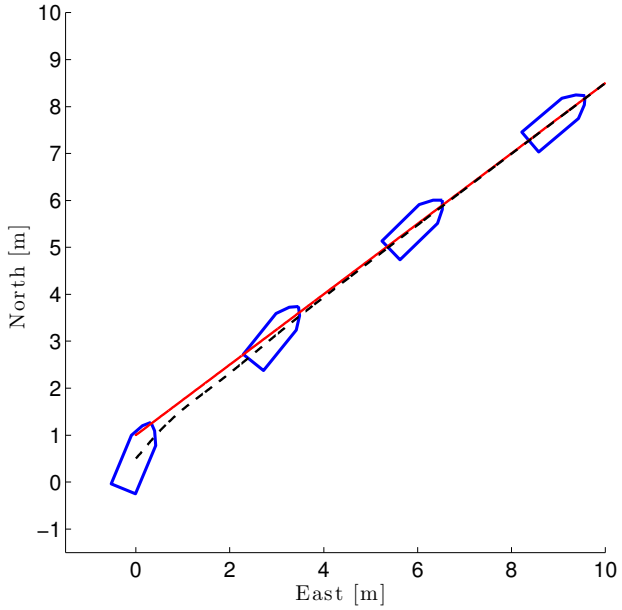

Fig. 2. Vessel tracing the desired straight-line path

A particular reason to why the $\mathcal{L}_1$ adaptive backstepping methods have a faster tracking performance is due to the choice of adaptation gains. The $\mathcal{L}_1$ adaptive backstepping then gets a tracking performance which is similar to the performance of a backstepping implemented to the vessel without the uncertainties and the disturbance.

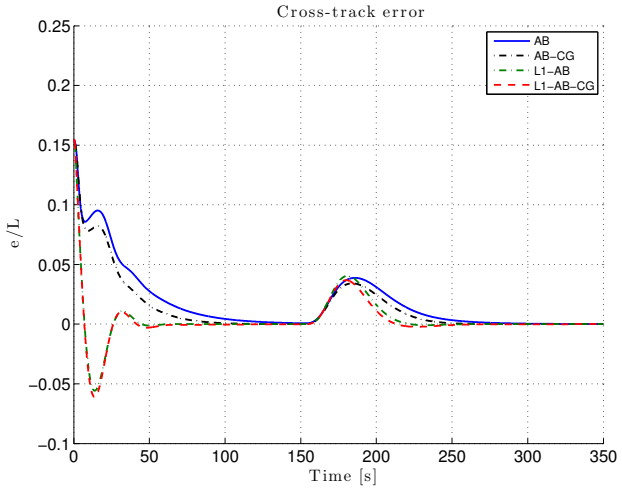

Fig. 3. The cross-track error scaled by the vessel length, in the straight-line motion scenario

The control signals are shown in Fig. 4. From this figure it is not possible to differentiate between the method with and without the command governor. However, there is a small difference between adaptive backstepping control and $\mathcal{L}_1$ adaptive backstepping control at the beginning.

Fig. 5 and 6 display the curves of IAE, ISE, ITAE and IAEW for the cross-track error. Both Fig 5 and 6 indicate that the $\mathcal{L}_1$ adaptive backstepping control methods have a better performance than the adaptive backstepping counterparts. Both IAE and ISE indicate that a command-governor improves the performance when the disturbance is introduced.

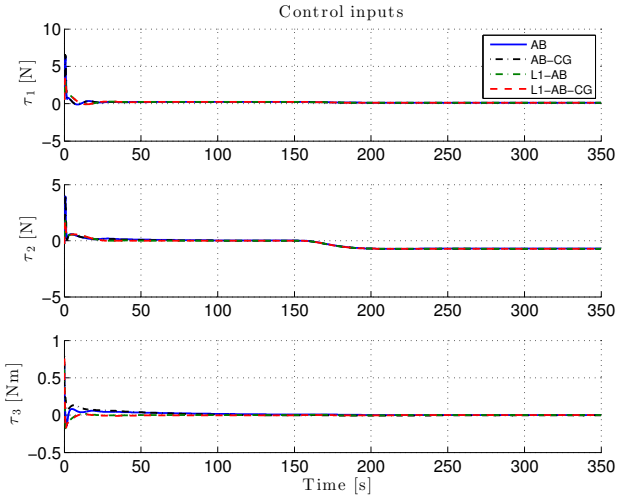

Fig. 4. The control inputs in the straight-line motion scenario

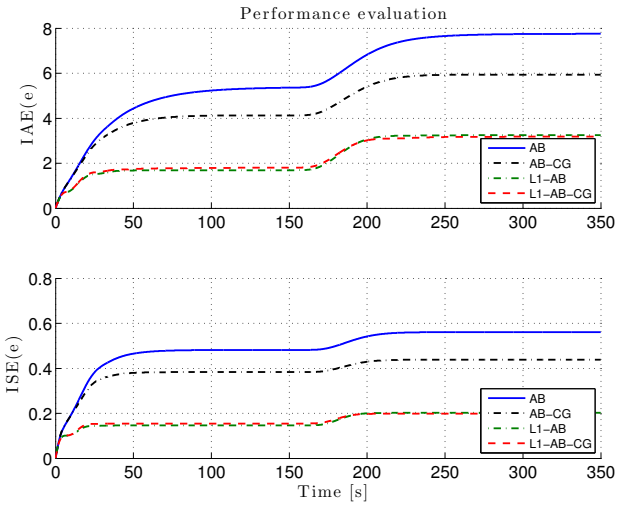

Fig. 5. The IAE and ISE of the cross-track error in the straight-line motion scenario

The ITAE displayed in Fig. 6a indicates that all the methods yield convergence of the cross-track error to zero. The plots of the IAEW illustrate that introducing the command governor improves the tracking performance versus energy consumption when a disturbance is affecting the system.

4.3 Results for Circular Motion

Here, motion control for a circular trajectory is considered. Note that this scenario does not satisfy the assumption about the uncertainty dynamics from Section 2, since the disturbance will get similar dynamics as the manoeuvring vessel.

For the circular motion, the reference pose $\boldsymbol{\eta}_d(t)$ is derived from

$$\boldsymbol{\eta}_p(t) = \left[x_p(t), y_p(t), \operatorname{atan2}\left(\dot{y}_p(t), \dot{x}_p(t)\right)\right]^\top,$$

where

$$x_p(t) = r_c \cos\left(\frac{\omega t}{r_c}\right), \quad y_p(t) = r_c \sin\left(\frac{\omega t}{r_c}\right),$$

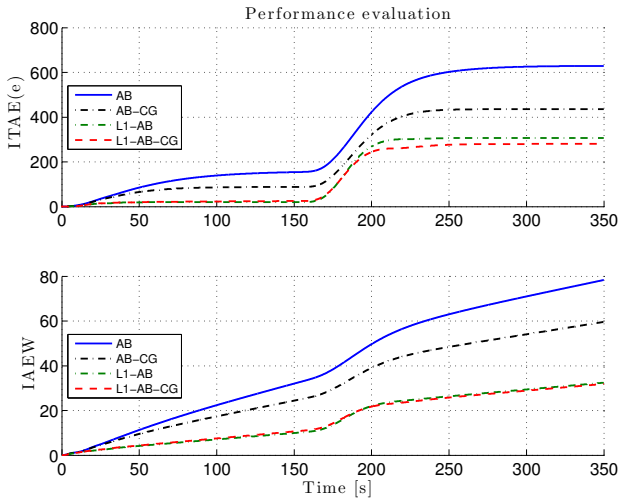

Fig. 6. The ITAE and IAEW of the cross-track error in the straight-line motion scenario

with speed $\omega = 0.15\ (m/s)$ and circle radius $r_c = 6\ (m)$. By applying $\boldsymbol{\eta}_p(t)$ to a third-order lowpass filter, we get $\boldsymbol{\eta}_d(t) \in \mathcal{C}^2$. The initial condition of the reference signal is chosen to be $\boldsymbol{\eta}_d(0) = [6\ (m), 0\ (m),\ 1.5708\ (rad)]^\top$, while the initial vessel states are chosen as $\boldsymbol{\eta}_0 = [5.5\ (m), 0\ (m),\ 1.5708\ (rad)]^\top$ and $\boldsymbol{\nu}_0 = [0\ (m/s), 0\ (m/s), 0\ (rad/s)]^\top$. The rest of the parameters are equivalent to those in Section 4.1.

Fig. 7 illustrates the desired and real trajectory of the vessel. The performance metrics are used to evaluate the performance of the different methods. Results are displayed in figures 8-11.

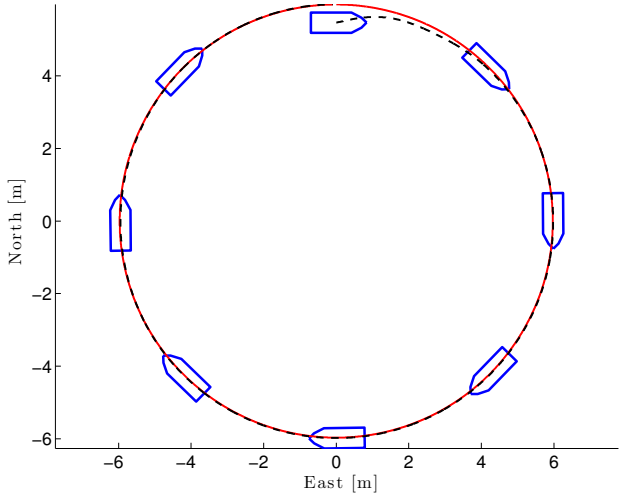

Fig. 7. Vessel tracing the desired circular path

The performance metrics give the same conclusion as they did for straight-line motion, which is that the $\mathcal{L}_1$ adaptive backstepping method is better than the adaptive backstepping methods, and that the transient is improved by combining the adaptive control method with a command governor. The growing ITAE indicates that there is a stationary error in performance of all the controllers, which is because of the assumption about the external disturbance is not satisfied for circular motion.

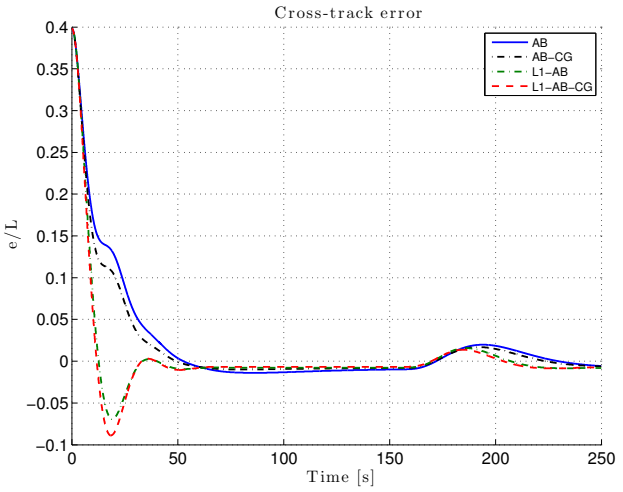

Fig. 8. The cross-track error scaled by the vessel length, in the circular motion scenario

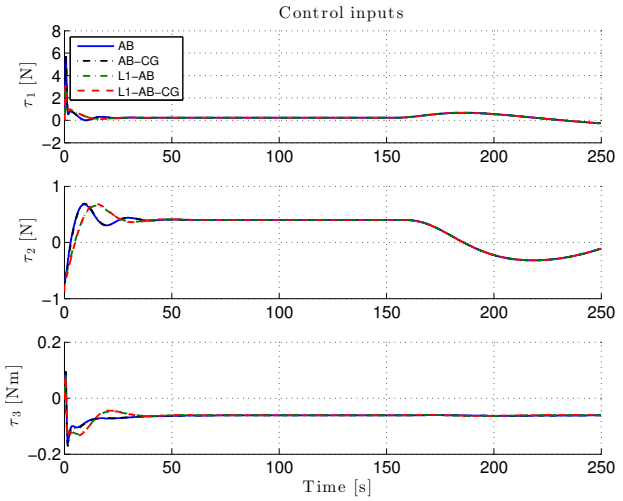

Fig. 9. The control inputs in the circular motion scenario

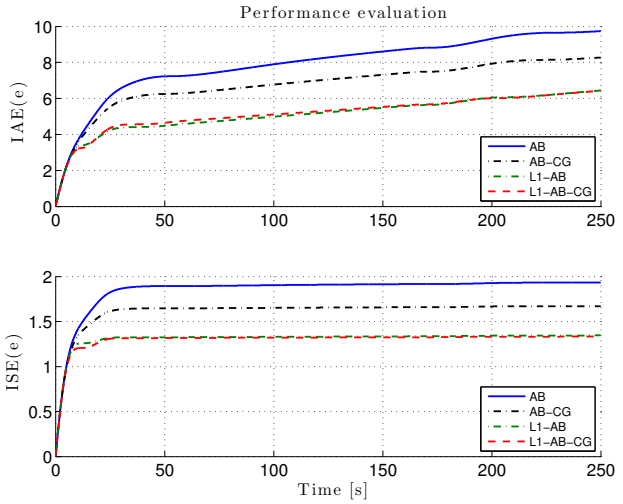

Fig. 10. The IAE and and ISE of the cross-track error in the circular motion scenario

5. CONCLUSION

We have presented the design of four control laws based on adaptive backstepping, $\mathcal{L}_1$ adaptive backstepping and the

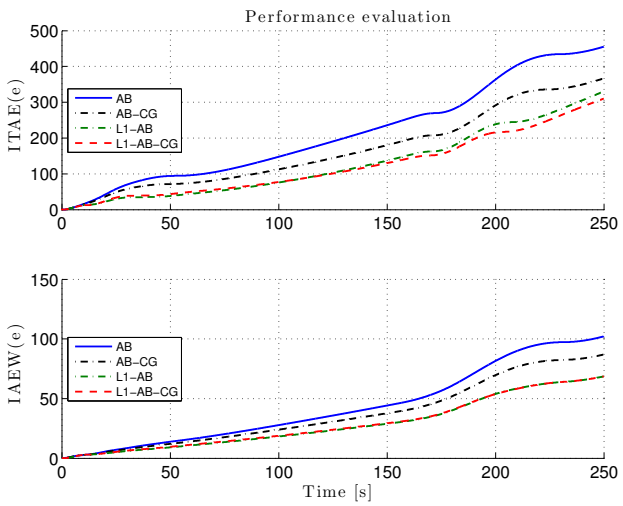

Fig. 11. The ITAE and IAEW of the cross-track error in the circular motion scenario

command governor concept, with the purpose of controlling the motion of a nonlinear 3 DOF model of a marine surface vessel. A comparative analysis of the methods have been made in order to find out which controller has the best performance. The simulation results have shown that all the considered controllers have good tracking performance and ability to compensate for internal and external uncertainties. However, utilising the benefit which $\mathcal{L}_1$ adaptive control gives, we are able to choose higher adaptation rates without encountering the problem of high-frequency oscillations in the control signal and therefore get a better tracking performance than for adaptive backstepping. Through the simulations, we have also observed that by combining an adaptive controller with a command governor, it is possible to improve transient performance.

Future work includes proving stability and robustness of the closed-loop adaptive systems. Additionally, it is desirable to experimentally verify the results by implementing the methods on a model-scale test vessel in a controlled environment.

ACKNOWLEDGEMENTS

This work was supported by the Research Council of Norway through the Centres of Excellence funding scheme, project number 223254.

REFERENCES

Bemporad, A. and Mosca, E. (1995). Nonlinear predictive reference governor for constrained control systems. *Proceedings of 34th IEEE Conference on Decision and Control, New Orleans, USA.*

Breu, D.A. and Fossen, T.I. (2011). $\mathcal{L}_1$ adaptive and extremum seeking control applied to roll parametric resonance in ships. *Proceedings of 9th IEEE International Conference on Control and Automation, Santiago, Chile.*

Fossen, T.I. (2011). *Handbook of Marine Craft Hydrodynamics and Motion Control.* Wiley.

Fossen, T.I. and Strand, J.P. (1999). Tutorial on nonlinear backstepping: Applications to ship control. *Modeling, Identification and Control*, vol. 20 (No. 2), pp. 83–135.

Hovakimyan, N. and Cao, C. (2010). *$\mathcal{L}1$ adaptive control theory: Guaranteed robustness with fast adaptation.* SIAM.

Krstic, M., Kanellakopoulos, I., and Kokotovic, P.V. (1995). *Nonlinear and adaptive control design.* Wiley.

Lee, C.H., Tahk, M.J., and Jun, B.E. (2012). Autopilot design for an agile missile using $\mathcal{L}_1$ adaptive backstepping control. *Proceedings of 28th Congress of the International Council of the Aeronautical Sciences, Brisbane, Australia.*

Patel, V.V., Wise, K.A., Hovakimyan, N., Cao, C., and Lavretsky, E. (2007). $\mathcal{L}_1$ adaptive controller for tailless unstable aircraft in the presence of unknown actuator failures. *Proceedings of AIAA Guidance, Navigation, and Control Conf., Hilton Head, South Carolina, USA.*

Ren, R., Zou, Z., and Wang, X. (2014). $\mathcal{L}_1$ adaptive control used in path following of surface ships. *Proceedings of 33rd Chinese Control Conference, Nanjing, China.*

Schatz, P., Yucelen, T., and Johnson, E.N. (2013). Constrained adaptive control with transient and steady-state performance guarantees. *Proceedings of CEAS EuroGNC, Delft, Netherlands.*

Skjetne, R., Smogeli, Ø.N., and Fossen, T.I. (2004). Nonlinear ship manoeuvering model: Identification and adaptive control with experiments for a model ship. *Modeling, Identification and Control*, vol. 25 (No. 1), pp. 3–27.

Svendsen, C.H., Holck, N.O., Galeazzi, R., and Blanke, M. (2012). $\mathcal{L}_1$ adaptive manoeuvring control of unmanned high-speed water craft. *Proceedings of 9th IFAC Conference on Manoeuvring and Control of Marine Craft, Arenzano, Italy.*

Theisen, L.R.S., Galeazzi, R., and Blanke, M. (2013). Unmanned water craft identification and adaptive control in low-speed and reversing regions. *Proceedings of 9th IFAC Conference on Control Applications in Marine Systems, Osaka, Japan.*

Yucelen, T. and Johnson, E. (2012a). Command governor-based adaptive control. *Proceedings of AIAA Guidance, Navigation, and Control Conference, Minneapolis, USA.*

Yucelen, T. and Johnson, E. (2012b). Design and analysis of a novel command governor architecture for shaping the transient response of nonlinear uncertain dynamical systems. *Proceedings of 51st IEEE Conference on Decision and Control, Maui, USA.*